

CONTROL OF RUPTURE BY FAULT GEOMETRY DURING THE 1966 PARKFIELD EARTHQUAKE

BY ALLAN G. LINDH AND DAVID M. BOORE

ABSTRACT

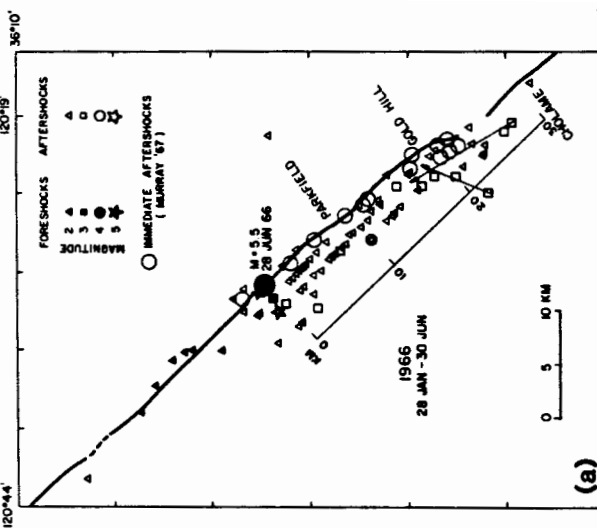
A reanalysis of the available data for the 1966 Parkfield, California, earthquake ($M_L = 5\frac{1}{2}$) suggests that although the ground breakage and aftershocks extended about 40 km along the San Andreas Fault, the initial dynamic rupture was only 20 to 25 km in length. The foreshocks and the point of initiation of the main event locate at a small bend in the mapped trace of the fault. Detailed analysis of the P-wave first motions from these events at the Gold Hill station, 20 km southeast, indicates that the bend in the fault extends to depth and apparently represents a physical discontinuity on the fault plane. Other evidence suggests that this discontinuity plays an important part in the recurrence of similar magnitude 5 to 6 earthquakes at Parkfield.

Analysis of the strong-motion records suggests that the rupture stopped at another discontinuity in the fault plane, an en-echelon offset near Gold Hill that lies at the boundary on the San Andreas Fault between the zone of aseismic slip and the locked zone on which the great 1857 earthquake occurred. Foreshocks to the 1857 earthquake occurred in this area (Sieh, 1978), and the epicenter of the main shock may have coincided with the offset zone. If it did, a detailed study of the geological and geophysical character of the region might be rewarding in terms of understanding how and why great earthquakes initiate where they do.

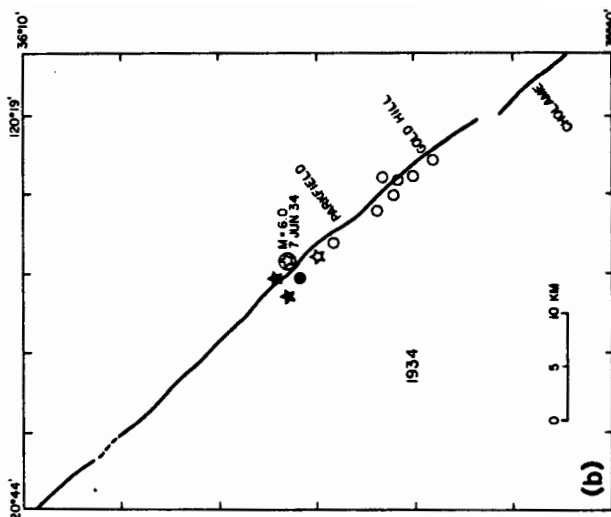
INTRODUCTION

In late 1965, five three-component accelerographs were installed in an array across the San Andreas Fault near Cholame, California (Figure 1). On-scale records were obtained at all these stations for a moderate earthquake ($M_L = 5.5$, $m_b = 5.9$, $M_S = 6.5$; Wu, 1968) that occurred on 28 June 1966, with the epicenter near Parkfield, California (Cloud and Perez, 1967). At the time, these records represented the most complete set of near-fault records available for a single earthquake. Their value was enhanced by the large number of other geological and geophysical data available for the earthquake; at least 12 seismological interpretations of the strong-motion data have been published (references to most of the papers can be found in Aki, 1979). No consensus about the details of the faulting has been reached, however. The published models can be grouped into three categories.

In the first group are those that have followed Aki (1968) in modeling only the record at station 2 (see Figure 1 for location). Their models fit the displacement (and in some cases the velocity) record with remarkable fidelity. This is not surprising, however, because these models have at least five free parameters of consequence (depth to top of dislocation, slip, rupture velocity, rise time, and the shape of the dislocation time-function) and only one record of simple shape to match. The models of this group fit the record at station 2 with slip on a fault plane passing almost directly beneath the station, ignoring the records at the other stations. As a consequence, the results obtained apply only to the shallow slip near Cholame and say nothing about the slip elsewhere on the fault. Another difficulty with many of these models is that they require on the order of 50 cm of slip at very shallow depths at the Highway 46 crossing near station 2; yet the morning following the earthquake, only $4\frac{1}{2}$ cm of surface slip had occurred at that point.



(a)

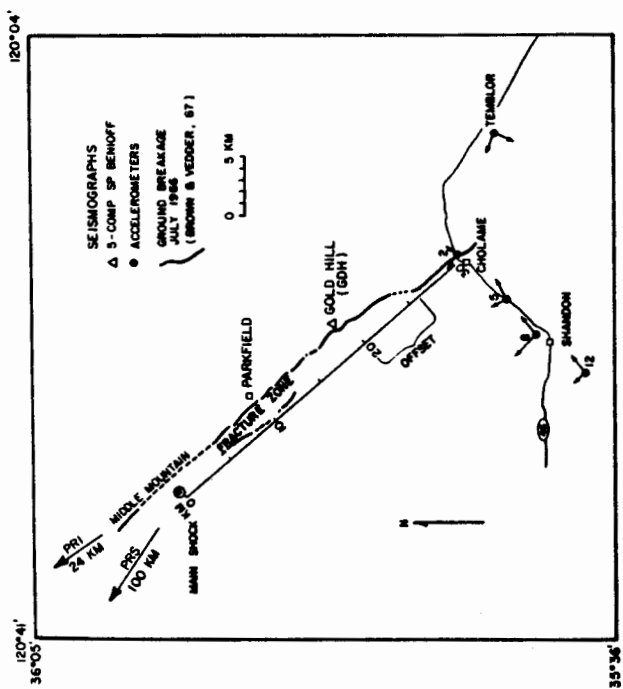


The unresolved question is the geometry of the initial rupture. Did it have roughly

Fig. 1. Map of Parkfield area showing ground breakage following the 1966 earthquake and seismic stations operating at that time. The distance scale shown is in kilometers along the fault southeast (positive) and northwest (negative) of the 1966 epicenter.

The second group of models follow Anderson (1974) in assuming an essentially uniform rupture whose areal extent approximately matches the aftershock zone (30 to 40 km in length between depths of 2 to 3 and 8 to 10 km). These models usually provide a reasonable fit to the shape and displacement amplitudes on all the records except those at station 2, where they underestimate the amplitude by a factor of 1.5 to 4. They also postulate extensive slip at depth in the region between Gold Hill and Cholame (Figure 1) where the geodetic data suggest that no deep slip occurred (Scholz *et al.*, 1969).

Related to the second group of models in spirit, but differing in two crucial aspects, is the work of Trifunac and Udwadia (1974), who divided the fault into seven segments and used a least-squares procedure to quantify the fit between the observed and calculated waveforms. They concluded that the data require about 120 cm of slip on a fault surface 20 km long stopping near Gold Hill, 10 km northwest of station 2. They also underestimated the station 2 displacement record by a factor of 2.



(a)

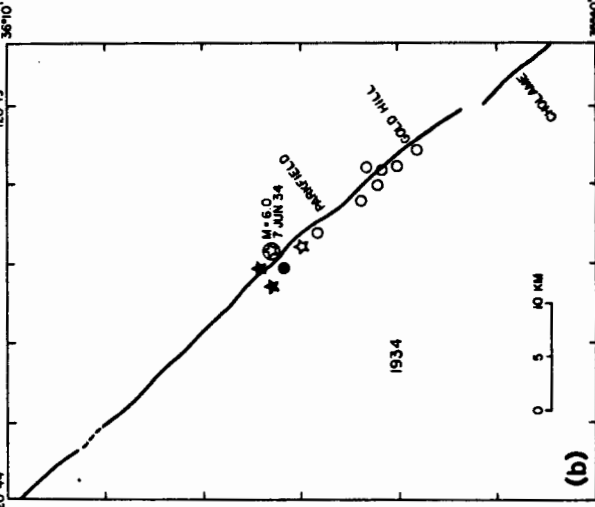


Fig. 2. (a) Map of Parkfield area showing location of the earthquakes of magnitude 2 and greater for the period 28 January 1966 thru 30 June 1966 (McEvily *et al.*, 1967). Locations of events south of Gold Hill are somewhat uncertain. For two such events (indicated by arrows), additional arrival times at Caltech stations imply locations at the heads of the arrows. Immediate aftershocks ($M \sim 3$ to 4) during the first 3 min after the main shock were located by Murray (1967) using P and S arrivals on the strong-motion array. (b) Foreshock and aftershock epicenter locations for the 1934 Parkfield earthquake (Wilson, 1936).

the length of the final aftershock zone and the zone of ground breakage, extending to Cholame, or did it have a shorter initial length, terminating south of Gold Hill where the early aftershocks concentrated (Figure 2a)? This is critical. The record at station 2 has different implications for the prediction of near-fault strong ground-motion if the rupture passes near the station than if it stops 5 to 10 km short of the station. Further, the interpretation of the strong-motion records in terms of the dynamics of the faulting processes depends on where the rupture stops, and important implications for fault mechanics are established if the rupture was terminated at the offset in the fault trace. Finally, the relation of the initial rupture to the ground breakage and the aftershock pattern is important, because these data are used to infer the rupture length for most earthquakes.

On the basis of P-wave first motions at the Gold Hill station and phase arrival times in the strong motion records, we will argue that the rupture length was less than inferred from the aftershock distribution and that the extent of faulting was controlled by two physical discontinuities on the San Andreas Fault: a small bend in the fault on Middle Mountain and the offset in the fault south of Gold Hill (Lindh and Boore, 1973, 1974).

SEISMICITY AND SLIP ASSOCIATED WITH THE PARKFIELD EARTHQUAKE

To provide background for discussion, here we will review some features of the earthquake before presenting our arguments. In what follows, we will refer often to the en-echelon offset in the surface trace of the San Andreas Fault near Gold Hill (Allen, 1969). For our purposes, we consider the offset to consist of the 6-km section of the active trace linking the two relatively straight segments northwest and southeast of Gold Hill (Figure 1). The points where the fault departs from these trends lie 20 and 26 km, respectively, southeast of the 1966 epicenter.

Seismicity. McEvilly *et al.* (1967) showed that while the 1966 Parkfield main shock was preceded by several months of seismic activity northwest of its epicenter, the rupture zone to the southeast was quiet at the magnitude 2 level (Figures 2a and 6). A sequence of foreshocks occurred during the final hours before the main event, the largest a magnitude 5 earthquake 18 min before the main shock. The location of the main epicenter, near the northwest end of the ground breakage and the aftershock distribution, implies unilateral rupture during the main shock to the southeast. The principal features of the aftershock distribution during the first 3 days were a cluster of events near the main epicenter and a nearly continuous distribution of epicenters at a somewhat lower density southeast to another cluster at Gold Hill (Figure 2a). During that time, no earthquakes were located north of the main epicenter and only a handful occurred south of the offset in the fault trace near Gold Hill. Wilson (1936) found a similar pattern of foreshocks and aftershocks accompanying the 1924 Parkfield earthquake, although he was able to locate only those of magnitude 4 and larger (Figure 2b). Note the similarity to the 1966 sequence, with foreshocks and main shock beneath Middle Mountain and aftershocks distributed for 20 km southeast of the epicenter, with a cluster near Gold Hill.

Eaton *et al.* (1970) used data from a dense array of portable short-period seismographs to obtain precise hypocentral locations for events during a 75-day period beginning 1 July 1966 (Figure 3). Precise locations (including good depth estimates) for a large number of small events allowed the detailed resolution of spatial features of the aftershock distribution. In particular, they showed that over most of the fault plane, the aftershocks occurred on a single vertical plane extending

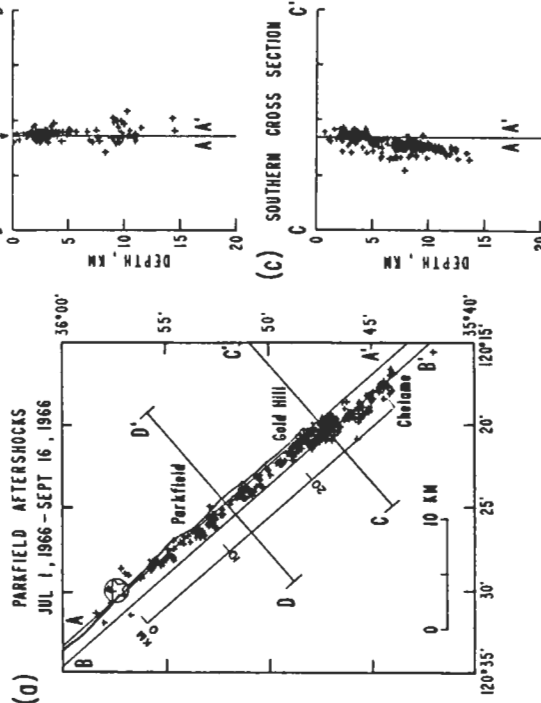


FIG. 3. (a) Map of Parkfield area showing well-located (A and B quality) aftershocks for the period 1 July to 15 September 1966 (Eaton *et al.*, 1970). (b) Transverse cross section of the northwest half of the data in (a). (c) Same as (b), southeast half.

from the surface to about 10-km depth and coinciding closely with the trace of the fault. Between 22 and 25 km south of Gold Hill (Figures 3 and 4), they found a right-stepping 1-km offset in the aftershock zone at depth that approximately corresponds to the en-echelon offset in the surface trace.

A longitudinal section along the main fault plane shows four concentrations of activity on the perimeter of the aftershock zone and very little activity in the central part (Figure 4a). In contrast, activity on the second plane, southeast of the offset, was concentrated almost entirely at the point where the two planes overlap. Only a sprinkling of small events ($M < 2$) are located south of that point (Figure 4b). A plot of seismic slip relative to distance along the fault, using these data and a moment magnitude relation from Bakun *et al.* (1976), shows two sharp peaks, one near the main event epicenter at the north, another at the en-echelon offset (Figure 5b). Similar plots of the aftershocks, relative to hypocentral depth, showed peaks at about 3- and 8-km depth (Eaton *et al.*, 1970; their Figure 19).

Surface slip. By extrapolations from direct measurement of offsets in geological and cultural features made the day following the earthquake, right-lateral surface slip of, at most, a few centimeters was inferred to have occurred at the time of the earthquake. As a result of afterslip, however, the total surface slip eventually reached 20 cm at points near the center of the fault break (Brown and Veevers, 1967). The afterslip, measured at several small geodetic figures, continued at a rate that decreased gradually after the earthquake (Wallace and Roth, 1967; Smith and Wyss, 1968). The distribution of slip along the Cholame Valley southeast of Parkfield was reasonably well defined by these measurements during July. They showed an

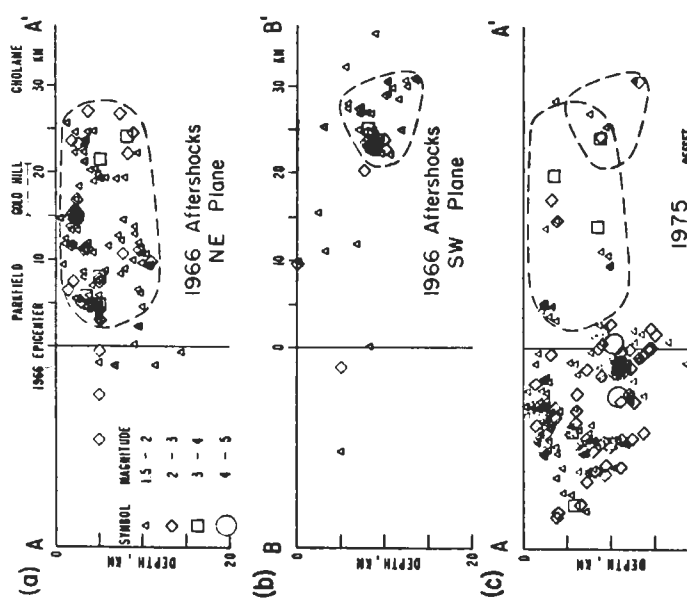


Fig. 4. Longitudinal cross section of aftershocks (A, B, and C quality, $M \geq 1.5$) along (a) the northeast side of the Cholame Valley, showing activity on the main fault plane that ruptured during the 1966 earthquake, and (b) the southwest side of Cholame Valley showing activity on the secondary fault plane southeast of Gold Hill. (c) Longitudinal cross section of earthquakes during 1975 located with same model used to obtain aftershock locations from (a) and (b) (dashed ellipses), the location of the 1966 epicenter (vertical line), the approximate extent of aftershock activity from (a) and (b) (dashed ellipses), the location of the en-echelon offset (triangles), and the uncertainty in the location of the source of the stopping phase (horizontal bar).

essentially linear decrease from Parkfield to the offset south of Gold Hill, with an additional short segment of slip between there and Cholame along the southwest side of the Valley (Figure 5c).

While the surface trace of the faulting is almost continuous between Gold Hill and Cholame where it crosses the valley (Figure 1), the geodetic and geological observations suggest that the slip went to zero at that point (Figure 5c). The aftershock distribution at depth suggests that the slip occurred on two separate planes that overlap one another by about 5 km at the offset (Figure 3). The data thus permit the interpretation, although they do not require it, that the principal slip at depth occurred on the main fault plane on the northeast side of the valley; that a small amount of sympathetic slip at depth occurred on the southwest strand south of Gold Hill; and that the surface slip in that area was an interpolation between the surface expression of two distinct fault segments at depth.

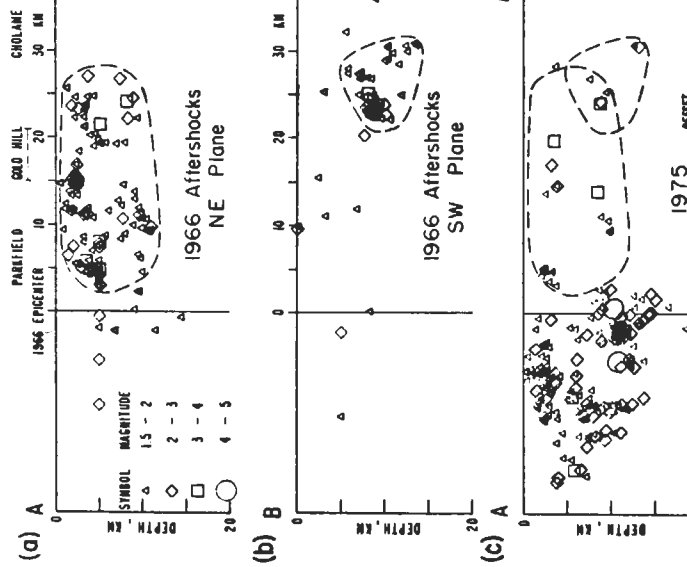


Fig. 5. (a) 1966 Epicenter and aftershocks in the Cholame Valley. (b) 1966 Aftershocks in the SW Plane. (c) 1975 Aftershocks in the NE Plane. Symbols represent different magnitude ranges: 1.5-2 (triangles), 2-3 (diamonds), 3-4 (squares), 4-5 (circles). A vertical dashed line marks the 1966 epicenter. A horizontal bar at the bottom indicates the en-echelon offset.

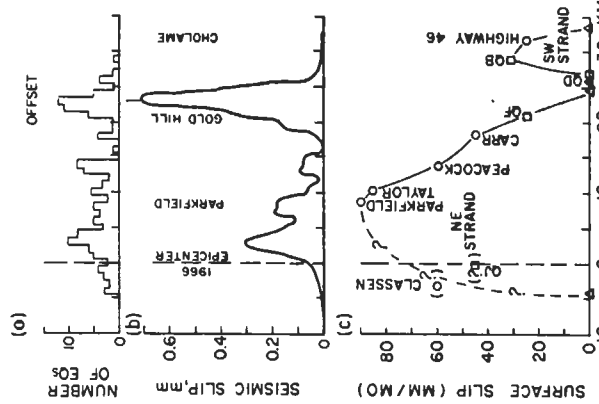


Fig. 6. (a) Number of aftershocks of $M \geq 1.5$ for the period 1 July thru 15 September 1966 (Raton *et al.*, 1970) plotted relative to distance along the fault. (b) Cumulative seismic slip for events in (a). Moment values for individual earthquakes were calculated using the relation $\log M_0 = 17 + 1.2 M$ (Bakun *et al.*, 1976) and the moments summed on 1-km intervals and converted to slip by the conventional relation $U = M_0 / uA$, where $u = 3 \times 10^{11}$ dyne/cm² and A is 1 km wide by 10 km deep. The plot was smoothed with a three-point running mean set that lateral resolution is 1 km. (c) Surface offsets along the San Andreas for July 1966. The northernmost points (between 0 and -5) are uncertain because of the difficulty in mapping on Middle Mountain and because the geodetic arrays were not installed there until late July and early August. The values shown for Qu and Classen are estimates obtained by extrapolating trends from a semi-log plot (displacement versus log time) back through July. □ Wallace and Roth (1967); ○ Smith and Wyss (1968); Δ, Brown and Wyss (1968); ▲, Brown and Veedor (1967). Shaded pattern and horizontal bar same as in Figure 4.

FORESHOCKS AND THE INITIATION OF RUPTURE

McEvilly *et al.* (1967) found that the immediate foreshocks were located very near the main epicenter (Figure 6). Epicentral locations for these foreshocks were controlled primarily by arrival times at two seismic stations, Priest Valley (PRI) to the north and Gold Hill (GDH) to the south (Figure 1). Thus, epicentral locations along the fault were reasonably well constrained, but depth and lateral position were not. We have used two independent types of evidence to infer that the foreshocks and main event were located along a 1-km stretch of the San Andreas Fault, the foreshock occurring northwest of the main shock.

Foreshock locations. If all the foreshocks on 26 June were located on the main trace of the San Andreas Fault, the arrival-time difference (Δt) between PRI and GDH is a direct measure of their relative location. This is very close to the method used by Wilson (1936) to obtain the foreshock and aftershock locations for the 1934 Parkfield sequence (Figure 2b) except that he used more distant stations in central

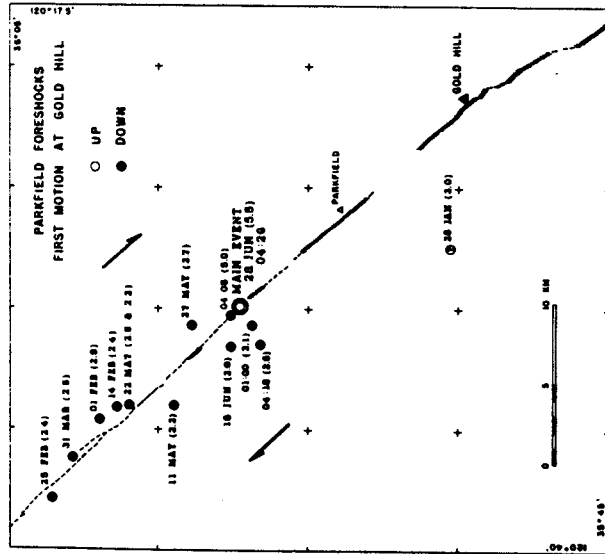


FIG. 6. Map showing Parkfield foreshock locations (locations from McEvilly *et al.*, 1967).

TABLE I
RELATIVE LOCATIONS OF FORESHOCKS AND MAIN SHOCK EXPRESSED BY RELATIVE P ARRIVALS AT
PARKFIELD AND GOLD HILL

Date	Time (UTC)	M _r	Arrival Times (sec)		PRI-GDH	PRI
			t	t + cc		
66 06 28	0100	3.1	63.5	-27.86	35.6	36.9
66 06 28	0114	1.8	87.0	-27.87	59.1	60.4
66 06 28	0408	5.1	88.4	-27.99	60.4	61.5
66 06 28	0418	2.6	65.25	-27.99	38.26	39.4
66 06 28	0426	5.5	45.4	-28.00	17.4	18.9

* McEvilly *et al.*, 1967.

† t_o, observed arrival times averaged from vertical and radial horizontal components; cc, clock correction; t, arrival times corrected for clock correction. Compare with times under PRI heading.
‡ McEvilly, personal communication, 1979. Clock corrections have been included.

and southern California. The time differences (Δt) between PRI and GDH are tabulated in Table I. The first two foreshocks appear to locate a few hundred meters northwest of the main shock epicenter, the next two another few hundred meters northwest (Figure 7).

Foreshock first motions. The polarities of P-wave first motions on the vertical 1-Hz Benioff seismometer at GDH show a pattern of dilatation for the foreshocks, compression for the main event (Figure 6), although McEvilly *et al.* (1967) reported

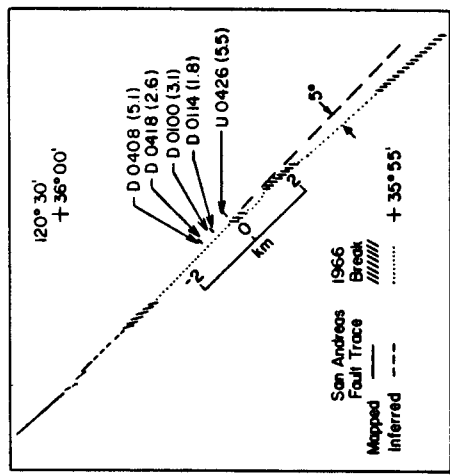


FIG. 7. Detail of the portion of the fault near the 1966 epicenter. Locations shown for the main event and the foreshocks are relocations obtained by constraining the earthquakes to lie on the fault and using the arrival times in Table 1. D, U represent the polarity of the events at Gold Hill and the four numerals give the hour and minute of the origin time.

that the large foreshock ($M_r = 5.1$) had the same radiation pattern as the main shock. Further, polarities at GDH of every well-located aftershock listed by Eaton *et al.* (1970), show dilatations for epicenters north of the foreshock-main shock region and compressions for epicenters to the south (Figure 8a). This pattern confirms that the foreshocks were located slightly northwest of the main shock, and rules out temporal variations as the explanation for the difference in polarity between the foreshocks and main shock.

The most obvious explanation for the polarity differences is a change in the orientation of the fault plane. Since station GDH lies close to a node in the expected P-wave radiation pattern for a double-couple point source, only a small rotation in fault-plane orientation would be required. In Figure 7 we show in detail the San Andreas Fault near the main shock epicenter (Brown, 1970). A small (5°) but distinct change in strike occurs in the trace at the location of the main shock epicenter. If the fault trace northwest of the epicenter is extrapolated southeast to GDH, that station would be in a compressional quadrant for earthquakes south of the bend of the fault but in a dilatational quadrant for events north of it (Figure 8b). Another possible explanation for the change in polarity at GDH is lateral refraction of the waves in the higher velocity material to the southwest of the fault. The phenomenon of lateral refraction is well established along the San Andreas Fault (e.g., McNally and McEvilly, 1977; Lindh *et al.*, 1978). If this phenomenon was controlling first motions at GDH, then the distance from the main shock location to GDH must be a crossover distance between direct waves and laterally refracted rays. We tested this hypothesis by studying first motions at a temporary seismic station and the more recent permanent station at Parkfield. As these stations are approximately equidistant between the main shock location and GDH, if the concept of a crossover distance were valid, then the first motions at these stations would be compressional for foreshocks immediately northwest of the main shock. Instead,

the distribution of polarities was the same as for the polarities at GDH (Figure 8b). This eliminates the hypothesis that the observed first-motion pattern is produced by lateral refraction and we conclude that the immediate foreshocks occurred northwest of a small bend in the fault, whereas the main event initiated just south of this same bend.

Bakun and McEvilly (1979) found that the frequency content of the magnitude 5 foreshock recorded on Wood-Anderson seismographs in both directions along the fault (at Berkeley and Mount Hamilton to the northwest, and at Santa Barbara to the southeast) required that the foreshock propagated unilaterally northwest, away from the bend in the fault. This contrasts with the main event, which clearly propagated southeast from the bend.

Further supporting evidence for a discontinuity at depth beneath the 1966 main shock epicenter is found in the pattern of seismicity and creep since 1966. Since 1971, the USGS has operated five short-period seismic stations in the Parkfield area. We adapted the crustal model and station corrections of Eaton *et al.* (1970) to this station set to relocate earthquakes in the area during 1975 (see the cross section in Figure 4c). The level of seismicity within the 1966 aftershock zone, with an average of 10 earthquake/yr ($M \geq 2$) and a b slope of -0.8 , is lower than on a comparable length of fault northwest of the bend, where the rate is threefold higher but has a b slope of -1.2 (Buhr and Lindh, unpublished data, 1980). In addition, the activity south of the bend is concentrated within a few clusters, whereas activity to the north is diffuse and somewhat shallower. Finally, a change in the long-term surface-slip pattern occurs near the main shock epicenter (Burford and Harrah, 1980).

The bend in the fault trace near the foreshock and main shock epicenters clearly coincides with a change in the nature of both seismic and aseismic slip on the fault. This bend might correspond to a discontinuity at depth on the fault, a possible cause of the change in background seismicity along the fault and the site of a local concentration of strain that is released in occasional larger earthquakes, such as that in 1966. If this is true, then the foreshocks represent concentration of stress at this point, with the main event initiated when the piled up dislocations spill through to the southeast.

THE ONSET OF RUPTURE TERMINATION

The records written by the five strong-motion instruments near Cholame contain a great deal of information concerning the details of the rupture of the 1966 event. No consensus has emerged concerning their interpretation, however. This situation has resulted from two inherent deficiencies of the records: first, each instrument was independently triggered and recorded no radio time signal, effectively making the trigger time of each instrument (and thus the arrival times of any phases) a free parameter in the modeling; second, all of the instruments were deployed in a linear array transverse to the fault at the extreme southern end of the subsequent faulting (Figure 1), making the calculated ground motion sensitive to the southernmost extent of faulting and insensitive to slip near the epicenter.

S arrivals and a common time base. We will first establish a common time base by identifying one phase-arrival on all instruments. The main difficulty with identifying discrete phases on the strong-motion accelerograms is the presence of a large

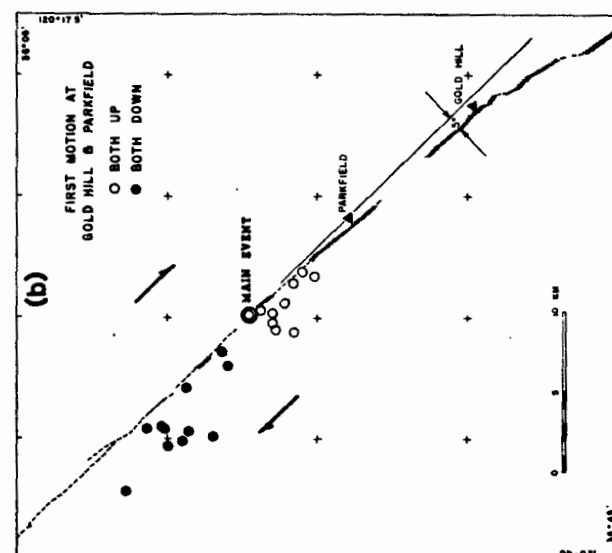
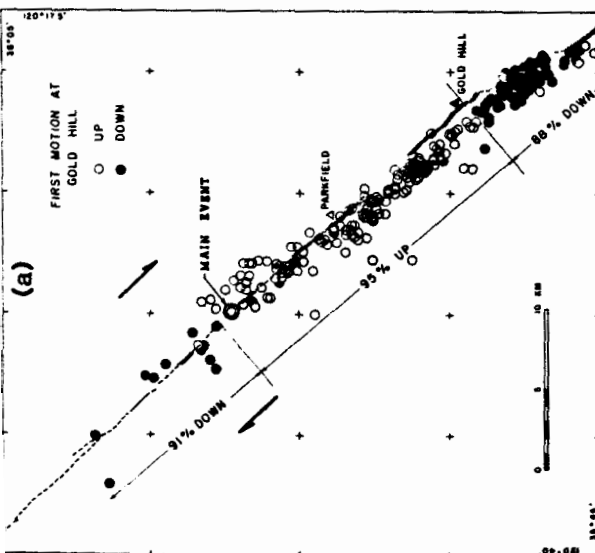


FIG. 8. (a) Map showing aftershock locations from Eaton *et al.* (1970). 91 per cent of events northwest of main epicenter have down first motions at Gold Hill. 96 per cent from there to Gold Hill are up; and 88 per cent south of that point are down. (b) Map showing first motions at PKF and GDH. Events are for a later time period than plotted in (a).

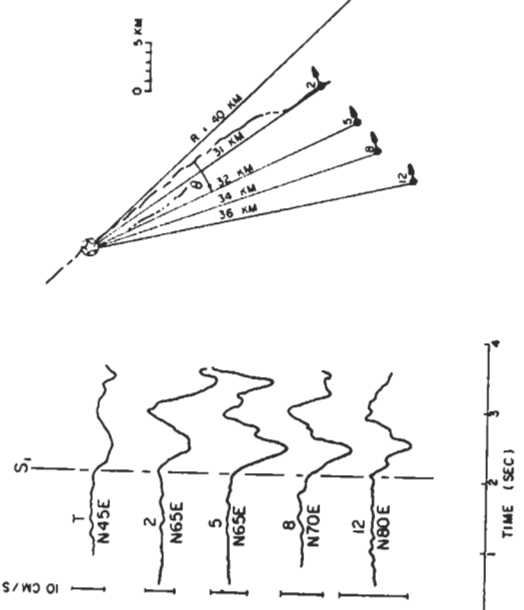


FIG. 9. Portions of the horizontal-velocity records at the five strong-motion instruments. Traces have been rotated to enhance SH motion from the hypocenter; trace down corresponds to ground motion in the labeled direction (see figure on right). The records are aligned by the first clear arrival on each, which we interpret as the starting phase, or S_1 , arrival from the epicentral end of the fault. Amplitudes are scaled by a factor of $R/\text{cav}^{2/3}$ to allow for the first-order effects of geometric spreading and radiation pattern.

amount of high-frequency energy throughout the records, presumably produced by short-wavelength heterogeneities in the faulting processes and/or the crustal structure through which the radiated energy propagates. This situation is improved somewhat if we look instead at the velocity records, whose low-frequency components have, in effect, been enhanced by a factor of $1/\omega$. A portion of the transverse horizontal-velocity components is shown in Figure 9, where the records are aligned on the first clear arrival on each trace. This pulse is interpreted as the direct shear-wave arrival from the epicenter, hereinafter called S_1 . In addition to their similar appearance, the S_1 arrivals have the appropriate first motion for an SH arrival from a right-lateral strike-slip rupture to the northwest and have roughly the amplitude variation with azimuth expected. The low amplitude at Temblor is probably a result of propagation through lower Q material on the east side of the fault (the average Q would have to be about one-half that on the west side of the fault).

The identification of the S_1 phase allows us to calculate the trigger time for each instrument relative to the origin time of the earthquake. The only additional information needed is an S-wave travel-time curve. Eaton *et al.* (1970) used a series of short refraction lines (Stewart and O'Neill, 1972) to derive layered crustal models for each side of the fault near Parkfield. We extended their work to S velocities by using arrivals from aftershocks recorded on three-component portable seismographs deployed by the U.S. Geological Survey in July of 1966. The S arrivals were modeled satisfactorily by using the P -velocity models of Eaton *et al.* (1970) with a V_p/V_s ratio of 1.73 to the southwest side of the San Andreas and 1.78 to the northeast (Boore and Lindh, unpublished data, 1974). For the epicentral distances, source

depths, and timing precision to be considered here, all the P -travel times can be approximated by using

$$t = 0.9 + \Delta/6$$

where Δ is the epicentral distance in kilometers. The S times are adequately given by multiplying the P time by 1.73. Using this relation and the S_1 arrivals in Figure 9, we have calculated trigger times (TT) for each of the five strong-motion instruments (Table 2), listed in seconds following the origin time of McEvilly *et al.* (1967), whose epicentral coordinates also were used. The only observations in the left side of Table 2 are the $(S_1 - TT)$ times from Figure 9.

The strongest evidence that these trigger times are essentially correct is the agreement between the calculated trigger time and the calculated arrival time of the P wave from the epicenter (P_1) at station 5. Because this instrument was found after the earthquake to have a "hair trigger" (Cloud and Perez, 1967), it is reasonable that it would have triggered on the first P arrival.

S arrivals from the vicinity of Gold Hill. Propagating shear dislocations radiate in the far field from any point on the fault plane at which sudden changes occur in the dislocation amplitude or rupture velocity. In particular, for a long narrow unilateral rupture, strong radiation (the "stopping phase") is expected from the rupture termination (Savage, 1965). In practice, because of inadequate records, the existence of this phase has rarely (if ever) been convincingly demonstrated. We believe we can do this for the 1966 Parkfield earthquake.

The dominant arrivals on the accelerograms are the large shear pulses on the horizontal components at stations 2, 5, 8, and Temblor (S_2) in Figure 10. When aligned, these large arrivals appear coherent, which suggests they could be treated as discrete phase arrivals. When the vertical components are similarly arranged, stations 2, 5, 8, and perhaps 12, have corresponding high-frequency phases (P_2 in Figure 11) with offsets from S_2 roughly proportional to the distance of the station from Gold Hill.

To test the hypothesis that these arrivals were P and S phases radiated from a

TABLE 2

STRONG-MOTION PHASE ARRIVAL TIMES

Station	Starting Phase*						Stopping Phase†					
	Δ_1 (km)	P_1 (sec)	S_1 (sec)	$(S_1 - TT)$ (sec)	TT (sec)	Δ_2 (km)	P_2 (sec)	S_2 (sec)	Δ_3 (sec)	P_3 (sec)	S_3 (sec)	Δ_4 (sec)
2	31.0	6.1	10.5	1.6	8.9	12.9	10.5	0.15	12.5	-0.08		
5	32.3	6.3	10.9	4.6	6.3	15.3	10.6	-0.15	13.27			
8	33.6	6.5	11.2	1.3	9.9	17.8	11.4	0.23	13.7	-0.29		
12	36.0	6.9	11.9	2.0	9.9	21.9	11.90	0.23	15.0	-0.17		
7	40.1	7.6	13.1	1.2	11.9	22.1	11.8	15.5	15.5	0.27		

* Δ_1 , distance from epicenter to station; P_1 and S_1 , calculated arrival times based on $P_1 = 0.9 + \Delta/6$ and $S_1 = 1.73 P_1$; $(S_1 - TT)$, observed S minus trigger time (underlined indicates that it represents a measurement); TT , derived trigger time obtained by subtracting column 5 from column 4, P_1 , S_1 , and TT are referenced to the origin time of the earthquake.

† Δ_2 , distance from derived origin of the S_2 ; phase near Gold Hill (18 km along the fault); this location corresponds to the minimum residual in Figure 12; the stations, P_2 , and S_2 , travel times between the stations and the origin near Gold Hill, referenced to the origin time of the earthquake. Values underlined were obtained by adding the observed phase-minus-trigger time to the trigger time in column 6; times otherwise calculated using the equations in note 1 and the inferred time difference between the origin of the phases 1 and 2 (7.3 sec). The Δ_3 columns are the residuals between the observed and calculated arrival times.

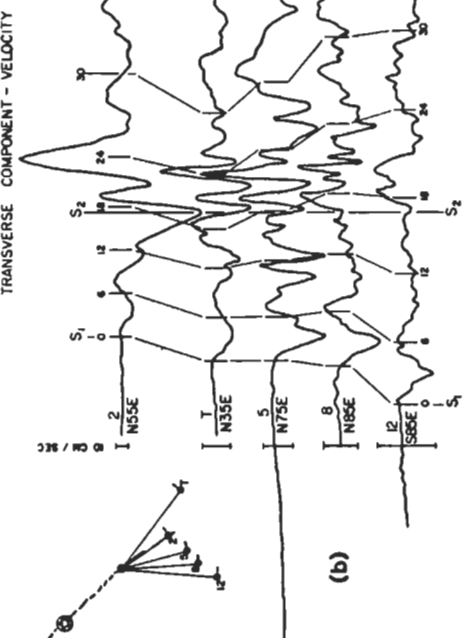
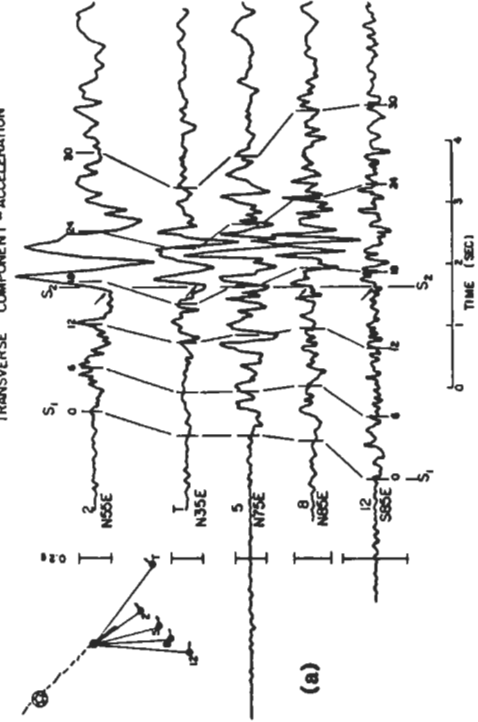


FIG. 10. Horizontal arrival for acceleration (a) and velocity (b) traces at the strong-motion stations, rotated into the SH direction for waves coming from a point near Gold Hill (see inset). Arrivals are aligned on S₂, a high-frequency arrival (arrow) or its calculated arrival time at station 3. Light vertical lines labeled 0, 6, 12, and so on indicate the times at which S arrivals would be expected from the indicated distances (in kilometers, see scale in Figure 1) along the fault based on our solution for the "stopping phase" (Table 2) and average rupture velocity (2.5 km/sec, Figure 12).

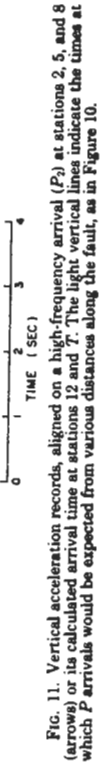


FIG. 11. Vertical acceleration records, aligned on a high-frequency arrival (P₂) at stations 2, 5, and 8 (arrows) or its calculated arrival time at stations 12 and 7. The light vertical lines indicate the times at which P arrivals would be expected from various distances along the fault, as in Figure 10.

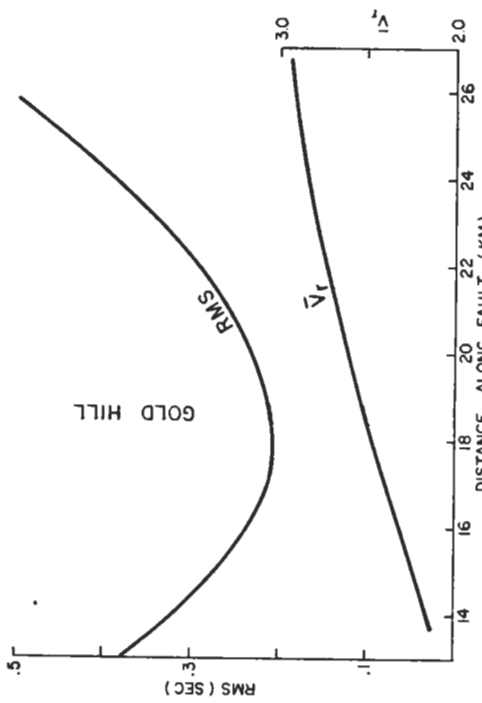


FIG. 12. Upper: rms fit of the observed travel times P_i and S_i (listed in Table 2). Lower: the average rupture velocity, V_r, for sources at various distances along the fault.

single point on the fault, we timed seven clear arrivals (the underlined numbers in columns P_2 and S_2 on the right side of Table 2; the arrivals denoted with arrows in Figures 10 and 11) and used them to locate the point on the fault from which they originated. The resulting travel-time residuals for the best-fitting location are also listed in Table 2. In Figure 12, the rms fit for the solution is plotted as a function of distance along the fault. A close study of the phases picked in Figures 10 and 11 and the residuals shown in Table 2 turns up several instances where with hindsight one could make "better" picks and reduce the rms considerably. For obvious reasons, we avoided this temptation. The picks shown were made on the basis of a careful study of the acceleration and velocity records and do not reflect any feedback from the calculated residuals. The minimum at 18 km corresponds to a location near Gold Hill. An estimated uncertainty of 0.1 sec in the phase arrival times corresponds to an uncertainty of about 4 km in the location of the stopping phase, resulting in a permissible range of 14 to 22 km. This range of permissible locations overlaps the offset in the fault trace (20 to 26 km, Figure 1), the offset in the aftershock distribution (22 to 26 km, Figure 3a), the end of the surface slip distribution along the NE strand of the fault (21 to 25 km, Figure 5c), and the southern peak in aftershock activity (20 to 25 km, Figures 4, a and b; 5, a and b). As all of these phenomena are evidence for heterogeneity in either the fault properties or the slip function (or both), we speculate that they are all related by an increase in the effective strength of a local region of the fault.

Whereas high-frequency arrivals are clear on the vertical components at stations 2, 5, and 8 (P_2 in Figure 11), the only significant vertical arrival at Temblor follows the S_2 arrival and is probably an SV phase. The calculated P_2 arrival time at Temblor, however, coincides with the calculated trigger time (see Table 2); i.e., the instrument was apparently triggered by the P_2 phase. Therefore, although the other stations were triggered by P arrivals from the epicenter (station 5) or points farther south along the fault (stations 2, 8, and 12), Temblor apparently did not trigger until the P_2 arrival. A source at Gold Hill, then, explains most of the large-amplitude arrivals recorded and accounts for the absence of an obvious P arrival at Temblor while explaining the instrument's trigger time.

We have emphasized the transverse horizontal components because radiation from strike-slip faulting is dominated by SH motion, particularly at small azimuths from the fault. However, 0.3 sec after the S_2 arrival, a coherent SV arrival is apparent at three stations (S_1 in Figure 13). It is larger than can be explained by strike-slip motion on a vertical fault, nor can it be accounted for by dip-slip or oblique-slip motion on a fault with the strike of the San Andreas, since the S_2 arrival is in-phase at stations 5 and Temblor, which lie in opposite quadrants. The simplest explanation entails dip-slip motion on a fault striking due north in the vicinity of Gold Hill (see the insert to Figure 13). Such a fault would tend to link up the two en-echelon segments of the San Andreas, and the sense of motion would be consistent with the long-term subsidence of the Cholame Valley.

Rupture velocity. The calculated origin time of the stopping phase (7.3 sec after the origin), taken with the 18-km length of break, gives an average rupture velocity to that point of 2.5 km/sec. Eaton (1967) estimated a rupture velocity of 2.2 km/sec, based on an arrival at 8.6 sec that he observed in the radio timing trace of the recording van at Gold Hill, near our stopping point. Since our estimate of 7.3 sec was calculated for a source at depth, some time must be added to allow for the propagation to the surface. Using Eaton et al.'s (1970) model for the northeast side of the fault and our measured V_p/V_s ratio of 1.8, we calculated the arrival times at

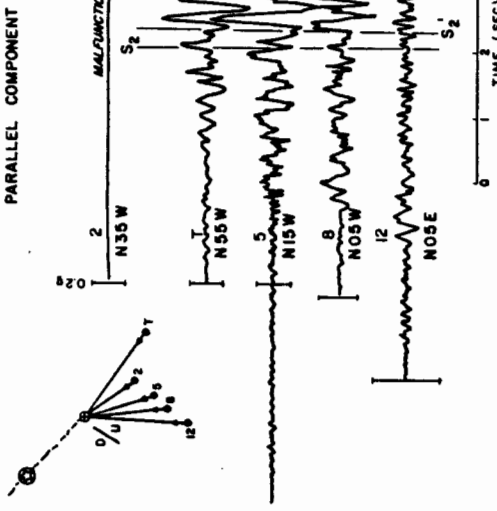


FIG. 13. Horizontal accelerograms rotated into the longitudinal (SM) component for S waves radiated from a point near Gold Hill, aligned as in Figure 10.

Gold Hill for a uniformly propagating source at a depth of 3 km, starting at the epicenter and propagating to the southeast with a rupture velocity of 2.5 km/sec. Most of the energy arrives at Gold Hill between 8.3 and 8.7 sec, in satisfactory agreement with Eaton's observation of 8.6 sec.

WHERE DID THE RUPTURE STOP?

The question remains, however, whether the large amplitude arrivals on the strong motion records came from near Gold Hill, as we have argued above, or whether the rupture continued to the southeast, on the southwest side of the valley. The latter hypothesis was first advanced by Aki (1968) who suggested that the high-frequency P arrivals (our P_2 phases) were radiated from the jog in the fault southeast of Gold Hill, but that the rupture continued on to station 2 and was responsible for the large amplitudes recorded there.

We recognize that the strong-motion record at station 2 is anomalous compared to the records at the other stations. In particular, the large shear arrival is of larger amplitude and longer period than expected from the character of the arrivals recorded at the other stations (Boore, 1974). We feel, however, that several lines of evidence argue against the rupture reaching Cholame. First, are the duration and amplitude of the large velocity pulses at stations 7, 5, 8, and 12. At most stations, for a rupture velocity of 2.5 km/sec there are no arrivals corresponding to fault lengths greater than 25 km (Figure 10b). (A fault length of 30 km is admissible only if the rupture velocity suddenly jumps to 3.4 km/sec southeast of the en-echelon offset. We consider this extremely unlikely.)

Another argument brings us to the same conclusion. A remarkable feature of the velocity records is their similarity at stations 5 and Temblor for 1 sec following the S_2 arrival (Figure 14). These two stations are located on opposite sides of the fault on different geological structures and are at different distances from Gold Hill.

During the S_2 arrival the peaks and troughs at station 5 and Temblor agree in time to better than 0.1 sec; this requires that the rupture producing these waveforms stopped at least 6 km north of Cholame. Arrivals from farther south would be delayed enough in reaching station 5 to destroy this observed coherence.

We have argued above that the high-frequency P_2 and S_2 arrivals on the strong motion records appear to come from near Gold Hill. In some cases, the S_2 waves also appear to have first motions appropriate to a stopping phase (i.e., opposite those of the S_1 phases). Of course, we located only the onset of this stopping phase. In reality, some finite distance is almost certainly required over which the displacement tapers to zero, and thus the stopping radiation would be expected over some time interval as the rupture comes to a halt. Madariaga (1975) has argued that for long, thin, strike-slip faults, the rise time, or duration of the source-time function, is approximately equal to the width of the fault divided by the shear wave velocity. In the absence of any clear observational or theoretical constraints, we can speculate that the distance over which the fault stops would be of the same order as the fault width, and that by analogy, the duration of the "stopping radiation" would be approximately equal to the rise time. At most stations, the largest acceleration and velocity amplitudes were recorded within 1/4 sec following the P_2 and S_2 arrivals (Figures 10 and 11); this time interval is comparable to the rise times estimated for fault widths of 5 to 10 km. The other phenomena we have associated with the termination of rupture (the southern extent of the larger aftershocks, the discontinuity in the surface fault trace, and the overlap in the aftershocks on the two fault strands) all have a scale length of about 5 km.

The model we tentatively propose then, for the termination of the Parkfield earthquake, is that the rupture began to stop at a point near Gold Hill, that the displacement tapered to zero within about 5 km, and that the stopping phase was radiated during the 1 to 2 sec this took to occur. This has the effect of giving a total fault length of about 25 km, which corresponds well to the total length of the aftershock activity on the northeast strand of the fault.

This interpretation also tends to minimize the discrepancy between our model and that of Aki (1968). We feel that modeling of the single horizontal record at station 2 is not sufficient to distinguish between fault lengths of 25 and 30 km and that the question of whether the rupture reached Cholame will only be resolved by modeling all the strong motion records, taking into account the phase arrival time constraints we developed in this paper. Realistic near-station crustal models will have to be used, particularly because station 2 lies within the zone of highly sheared, relatively low-velocity materials of the fault zone and is underlain by a greater

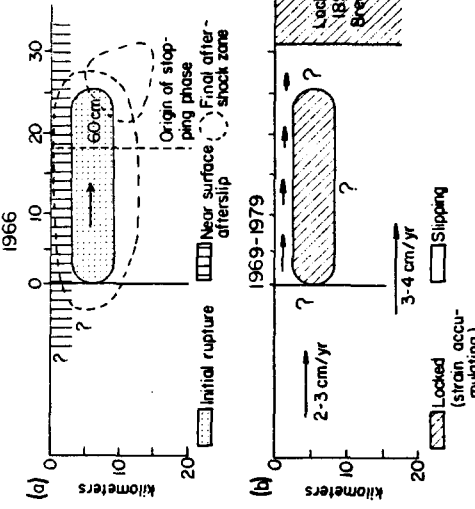


FIG. 15. Schematic cross sections of the San Andreas Fault in the Parkfield area showing our preferred model for the rupture during the 1966 earthquake (top) and for the strain accumulation phase between earthquakes (bottom).

thickness of unconsolidated to partially consolidated sediments than the other stations (W. B. Joyner, oral communication, 1979, based on velocity logs of wells and local refraction lines). These differences could lead to anomalous wave guide effects which might give the unique appearance of the record at station 2.

DISCUSSION

An unresolved question in earthquake mechanics is why earthquakes stop and/or why they occur on discrete patches of finite length. One possible explanation is a change in stress; i.e., they stop when they reach a region of lower tectonic stress. The other obvious possibility is that the extent of rupture is controlled by changes in strength produced by changes in the material properties in the fault zone and changes in the geometry of the fault such as bends or en-echelon offsets. It is very likely, of course, that both these processes contribute, and then it is a question of which dominates at a particular time and place. As no means exist for reliably estimating the shear stress at seismic depths, one can only speculate on how large a part stress inhomogeneities play. The situation is somewhat better with regard to the second hypothesis, for while direct sampling of the fault-zone materials at depth is not possible at this time, some inferences concerning materials and geometry can be drawn from geological and seismic evidence.

In great trench earthquakes, many workers have noted that not only do they tend to recur in the same places but the rupture zones of many adjacent earthquakes are separated by discontinuities along the strike of the trench. Mogi (1968) observed in Japan that many adjacent ruptures were separated by transverse structural features such as faults, ridges, and trenches. A similar pattern had been observed in the Aleutians (Sykes, 1971; Kelleher, 1970) and in central America (Carr and Stoiber, 1977). Observations that may be related have been made for large strike-slip earthquakes on the Anatolian and San Andreas faults, where bifurcations and en-

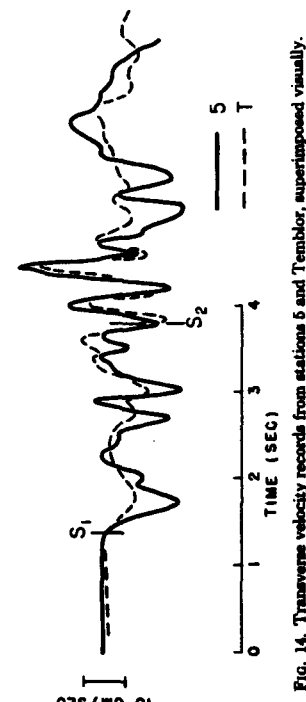


FIG. 14. Transverse velocity records from stations 5 and Temblor, superimposed visually.

echelon offsets bound the rupture zones of certain large earthquakes (Ambraseys, 1970; Allen 1968). In particular, Allen (1968) pointed out that the prominent en-echelon offset near Gold Hill may have formed the northern terminus of the 1857 Fort Tejon earthquake.

We have shown in this paper that the 1966 Parkfield earthquake started at a bend in the fault and stopped at the en-echelon offset near Gold Hill. These conclusions are summarized in Figure 15a, a schematic cross section of the San Andreas Fault in the Parkfield area. In Figure 15b, we have sketched one possible model for the strain accumulation that occurs between earthquakes. The principal feature of this model is a 5×25 -km stuck patch (Wesson *et al.*, 1973) centered on the 1966 aftershock zone, the source region of at least the last three Parkfield earthquakes (Bakun and McEvilly, 1979). It is adjoined to the northwest by an area of steady-state aseismic creep at 3 cm/yr (Burford and Harsh, 1980). Apparently aseismic slip at 3 to 4 cm/yr also occurs below 8 to 10 km depth, although we do not know whether this slip is steady-state or event-like, whether it lags or leads the slip on the shallower seismic zone, or at precisely what depth the transition occurs (Thatcher, 1979). The stuck patch is terminated to the southeast by the en-echelon offset south of Gold Hill and the locked portion of the fault that last failed during the 1857 Fort Tejon earthquake. This stretch shows no evidence of seismic or aseismic slip since that time and is assumed to be accumulating strain preparatory to the next great earthquake.

The stuck patch at Parkfield is transitional in two senses: spatially, in that it forms the boundary between the creeping and locked portions of the San Andreas, and temporally, in that it has moderate ($M \sim 5$) earthquakes at about 20-yr intervals. The correlation with the fault geometry is so striking that we believe it represents first-order evidence as to the mechanics of the fault. The picture we envision is strain accumulating at the bend as a result of the arrest of steady-state creep to the northwest by an increase in strength on the fault plane. When this point eventually fails, the piled-up dislocations propagate through to the next strong point on the fault, the en-echelon offset near Gold Hill. This has the effect, of course, of transferring strain to the locked portion of the San Andreas to the southeast.

Within this framework, the foreshocks in 1966 are presumed to have some direct link to the failure of the strong point at the bend, although we can only speculate as to whether the relation was one of cause or effect. By analogy, one could argue that the main event, in transferring an increment of stress to the locked portion to the south, was a potential Fort Tejon foreshock. Some credibility is lent this speculation by Sieh's observations that at least two magnitude 6 earthquakes did occur in the Parkfield area in the early hours of dawn just before the magnitude 8 Fort Tejon earthquake of 1857 (Sieh, 1978).

ACKNOWLEDGMENTS

We greatly appreciate our many conversations with William Joyner on this subject and thank W. H. Bakun and R. Archuleta for their critical comments and helpful suggestions concerning an early version of this paper. Grover Baehr and Ray Eis did the drafting and Virgo Barba patiently retypes the manuscript several times.

REFERENCES

- Aki, K. (1968). Seismic displacements near a fault. *J. Geophys. Res.* **73**, 5359-5376.
- Aki, K. (1979). Characterization of barriers on an earthquake fault. *J. Geophys. Res.* **84**, 6140-6148.
- Allen, C. R. (1968). The tectonic environments of seismically active and inactive areas along the San for Alaska and Aleutians. *J. Geophys. Res.* **74**, 8021-8041.
- Andreas Fault system. *Proceedings of the Conference on Geologic Problems of San Andreas Fault System, Stanford Univ. Publ. Geol. Sci.* **11**, 70-82.
- Allen, C. R. (1969). Active faulting in northern Turkey. *Contribution No. 157*, Div. of Geol. Sci., California Institute of Technology, Pasadena, California.
- Ambraseys, N. N. (1970). Some characteristic features of the Anatolian fault zone. *Tectonophysics* **8**, 143-165.
- Anderson, J. (1974). A dislocation model for the Parkfield earthquake. *Bull. Seism. Soc. Am.* **64**, 671-686.
- Bakun, W. H., C. G. Burford, and R. M. Stewart (1976). Body-wave spectra of central California earthquakes. *Bull. Seism. Soc. Am.* **66**, 383-394.
- Bakun, W. H. and T. V. McEvilly (1978). Earthquakes near Parkfield, California: comparing the 1934 and 1966 sequences. *Science* **204**, 1375-1377.
- Boore, D. M. (1971). Empirical and theoretical study of near-fault wave propagation. *Proceedings Sch. World Conf. Earthquake Eng.*, Rome, Italy, 1973, **2**, 2387-2406.
- Brown, R. D., Jr. (1970). Map showing recently active breaks along the San Andreas and related faults between the northern Gabilan Range and Cholame Valley, Calif., U.S. Geol. Surv., *Misc. Geol. Invest. Map I-75*.
- Brown, R. D., Jr. and J. G. Varder (1967). Surface tectonic fractures along the San Andreas fault, in U.S. Geol. Surv. *Profess. Paper* **779**, 2-23.
- Burford, R. O. and P. W. Harsh (1980). Results of alignment array surveys along the San Andreas fault in central California in relation to contemporary seismicity. *Bull. Seism. Soc. Am.* (in press).
- Carr, M. J. and R. E. Stoiber (1977). Geologic setting of some destructive earthquakes in Central America. *Bull. Geol. Soc. Am.* **88**, 151-166.
- Cloud, K. W. and R. Perez (1967). Accelerograms—Parkfield earthquake. *Bull. Seism. Soc. Am.* **57**, 1179-1192.
- Eaton, J. P. (1967). Instrumental seismic studies, the Parkfield-Cholame, California earthquakes of June-August, 1966. *U.S. Geol. Surv. Profess. Paper* **779**, 57-65.
- Eaton, J. P., M. E. O'Neill, and J. N. Murdoch (1970). Afterfocks of the 1966 Parkfield-Cholame, California earthquake: a detailed study. *Bull. Seism. Soc. Am.* **60**, 1161-1197.
- Kalleher, J. A. (1970). Space-time seismicity of the Alaska-Aleutian seismic zone. *J. Geophys. Res.* **75**, 5745-5756.
- Lindh, A. G. and D. M. Boore (1973). Another look at the Parkfield earthquake, using strong motion instruments as a seismic array (abstract). *Seism. Soc. Am. Ann. Mtg.*, Golden, Colorado, 16 pp.
- Lindh, A. G. and D. M. Boore (1974). The relation of the Parkfield foreshocks to the initiation and extent of rupture (abstract). *Earthquake Notes* **XLV**, 54.
- Lindh, A. G., D. A. Lockner, and W. H. K. Lee (1978). Velocity anomalies: an alternative explanation. *Bull. Seism. Soc. Am.* **68**, 721-732.
- Madariaga, R. (1976). Dependence of far-field radiation on source geometry. *EOS, Trans. Am. Geophys. Union* **57**, 40-40.
- McEvilly, T. V., W. H. Bakun, and K. B. Casady (1967). The Parkfield, California earthquakes of 1966, *Bull. Seism. Soc. Am.* **57**, 1221-1224.
- McEvilly, K. C. and T. V. McEvilly (1977). Velocity contrast across the San Andreas fault in central California: small scale variations from P-wave nodal plane distortion. *Bull. Seism. Soc. Am.* **67**, 1505-1516.
- Mogi, K. (1968). Relationship between the occurrence of great earthquakes and tectonic structures. *Bull. Earthquake Res. Inst., Tokyo Univ.* **47**, 429.
- Murray, G. S. (1967). Note on strong motion records from the June 1966 Parkfield, California earthquake sequence. *Bull. Seism. Soc. Am.* **57**, 1269-1266.
- Savage, J. C. (1965). The stopping phase on seismograms. *Bull. Seism. Soc. Am.* **55**, 47-58.
- Sieh, C. H., M. Wynn, and S. W. Smith (1968). Seismic and aseismic slip on the San Andreas fault, J. Geophys. Res. **74**, 2048-2059.
- Sieh, K. E. (1978). Central California foreshocks of the great 1867 earthquake. *Bull. Seism. Soc. Am.* **68**, 1731-1760.
- Smith, S. W. and M. Wynn (1968). Displacement on the San Andreas fault subsequent to the 1966 Parkfield earthquake. *Bull. Seism. Soc. Am.* **58**, 1865-1873.
- Stewart, S. W. and M. E. O'Neill (1972). Seismic traveltimes and near-surface crustal velocity structure bounding the San Andreas fault zone near Parkfield, California, U.S. Geological Surv. Profess. Paper **800-C**, C117-C125.

- Thatcher, W. (1979). Systematic inversion of geodetic data in central California, *J. Geophys. Res.* **84**, 2283-2295.
- Trifunac, M. D. and F. E. Udwadia (1974). Parkfield, California earthquake of June 27, 1966; a three-dimensional moving dislocation, *Bull. Seism. Soc. Am.* **64**, 511-534.
- Wallace, R. E. and E. F. Roth (1967). Rates and patterns of progressive deformation, in *The Parkfield-Cholame, California Earthquakes June-August 1966*, U.S. Geol. Surv. Profess. Paper 579 23-40.
- Wesson, R. L., R. O. Burford, and W. L. Ellsworth (1973). Relationship between seismicity, fault creep and crustal loading along the central San Andreas fault, *Proceedings of the Conference on Tectonic Problems of the San Andreas fault system, Stanford Univ. Publ. Geol. Sci.* **13**, 303-321.
- Wilson, J. T. (1936). Foreshocks and aftershocks of the Nevada earthquake of December 20, 1932 and the Parkfield earthquake of June 7, 1934, *Bull. Seism. Soc. Am.* **26**, 189.
- Wu, F. T. (1968). Parkfield earthquake of June 28, 1966: magnitude and source mechanism, *Bull. Seism. Soc. Am.* **58**, 689-709.

U.S. GEOLOGICAL SURVEY
345 MIDDLEFIELD ROAD, MS-77
MENLO PARK, CALIFORNIA 94025

DEPARTMENT OF GEOPHYSICS
STANFORD UNIVERSITY
STANFORD, CALIFORNIA 94305

Manuscript received June 3, 1980